

Copyright WILEY-VCH Verlag GmbH & Co. KGaA, 69469 Weinheim, Germany,
2010.

NANO MICRO
small

Supporting Information

for *Small*, DOI: 10.1002/smll. 201001916

Structured Graphene Devices for Mass Transport

Amelia Barreiro, Riccardo Rurali, Eduardo R. Hernández, and
Adrian Bachtold *

Supporting Information

1. Scanning electron microscopy of the motion

We present here the full series of recorded images of the devices shown in **Fig. 1 and 2** of the paper.

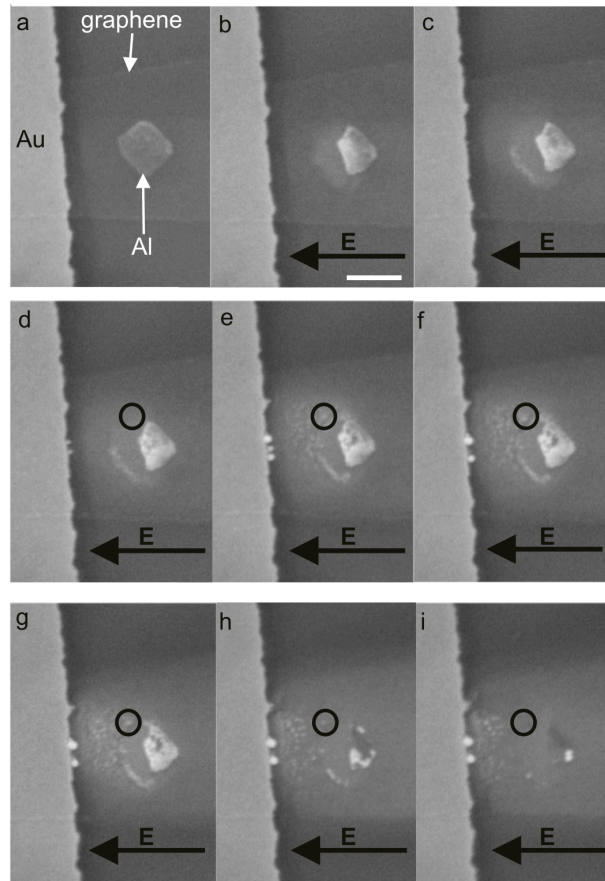


Figure S1. (a) Scanning electron microscopy image of a graphene device with one Al plate. The scale bar is 400 nm. (b-i) Motion of the aluminum after having applied an electric field. The arrow indicates the direction of the electric field. The black circle shows a piece of Al. Initially this piece grows with time, but eventually the growth process is reversed and the piece shrinks and disappears.

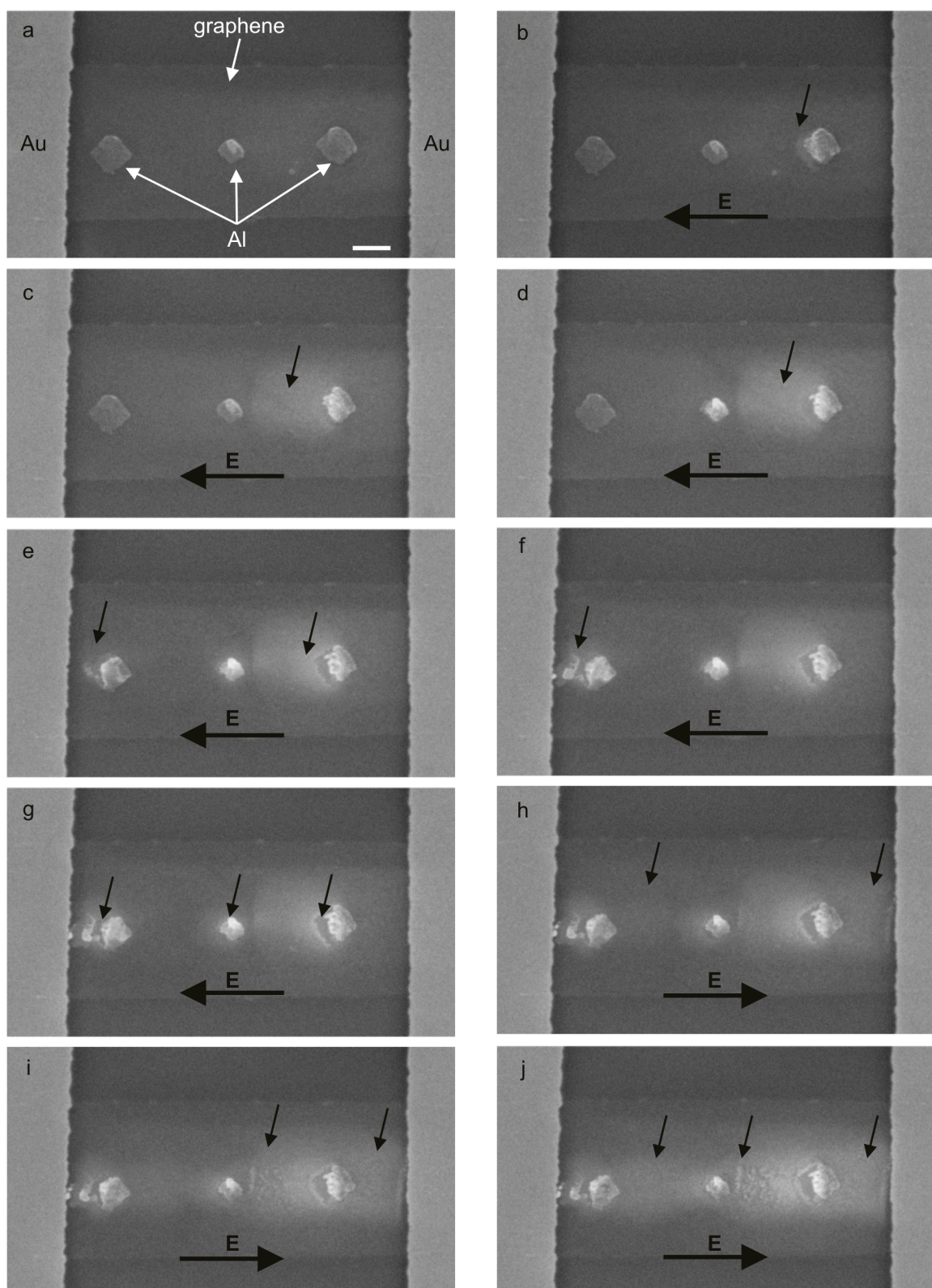


Figure S2. (a) Scanning electron microscopy image of a graphene ribbon contacted to two Au electrodes. Three square-shaped Al plates are lying on top of the graphene. The scale bar is 500 nm. (b-j) Motion of the aluminum after having applied an electric field (whose direction is indicated by the long arrow). The displacement is highlighted with short arrows.

2. Density-functional theory calculations

We have performed density-functional theory (DFT) calculations, using the SIESTA package.^{1,2} We have used a double- ζ basis set plus polarization functions for the valence electrons, while core electrons are accounted for by means of norm-conserving pseudopotentials of the Troullier-Martins type.^{3,4} The exchange-correlation energy is treated within the Generalized Gradient Approximation (GGA).⁵ We have used a computational cell made of 9×9 replicas of the graphene primitive cell; this supercell allowed us to sample the Brillouin zone with the Γ point only for the relaxations and is large enough to make negligible, at a first approximation, the interaction of the impurity with its periodic images. All the structures have been optimized until the force on the atoms were lower than 0.04 eV/\AA . A denser mesh of 10×10 \mathbf{k} -points has been used to refine the electronic structure of the minimum energy structures. Some geometries have also been relaxed with the VASP package, using a plane-wave cutoff of 400 eV for comparison.⁶ We have considered Al and Au impurities on a graphene sheet (see main text). For both impurities we have checked three different configurations, placing the impurity atom (i) above the center of a C-hexagon, (ii) above a C atom and (iii) above the bond center position of a C-C bond. All these three initial configurations lead to three different local minima after relaxation, where the distortions of the graphene layer go from negligible to minimal (0.2 \AA).

3. Conductance and force calculations

Following a common approach in this kind of calculations, the system is divided into three regions: a left lead, a right lead and a central scattering region containing the Al impurity. We solve the electronic structure problem in the central region with the TRANSIESTA method within the non-equilibrium Green's function formalism, where the open boundary conditions imposed by the electrodes are accounted for through the left (right) self-energy $\hat{\Sigma}_{L,R}(E)$.⁷ The

zero-bias transmission $T(E)$ is calculated using non-equilibrium Green's functions with the TRANSIESTA code as

$$T(E) = \text{Tr} \left[\hat{G}_C^r(E) \hat{\Gamma}_L(E) \hat{G}_C^a(E) \hat{\Gamma}_R(E) \right] \quad (1)$$

where $\hat{G}_C^{r,a}(E) = [E\hat{S}_C - \hat{H}_C - \hat{\Sigma}_L^{r,a}(E) - \hat{\Sigma}_R^{r,a}(E)]^{-1}$ is the retarded (advanced) Green's function of the scattering region and $\hat{\Gamma}_{L,R}(E) = i(\hat{\Sigma}_{L,R}^r - \hat{\Sigma}_{L,R}^a)$. The conductance G can now be calculated through the Landauer formula as

$$G = \frac{2e^2}{h} T(E) \quad (2)$$

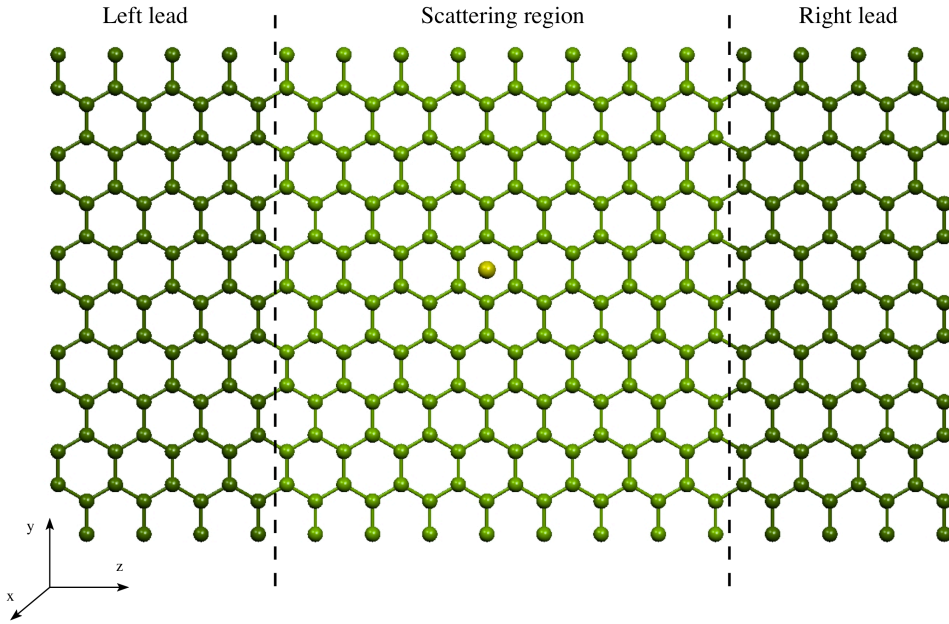


Figure S3. Supercell geometry employed in our conductance calculations. The central region with atoms highlighted in light green is the scattering region, where the impurity atom is located (shown in yellow); left and right leads have atoms shown in dark green.

As the transport calculations are computationally more demanding, we have used a reduced, but reliable single- ζ polarized basis set. A dense \mathbf{k} -point sampling in the direction perpendicular to the transport is required to obtain converged results of the transmission. We

have obtained converged results with 240 points in the k_{\parallel} direction. As an outcome of these calculations we also obtain the total force acting on the impurity atoms in the presence of a bias.⁸

4. Derivation of the Wind Force (Equation 1 of main text)

In what follows we adopt atomic units, in which $\hbar = 1$ and \bar{k} has dimensions of momentum. Our starting expression is Eq. (22) in the paper by Sorbello, which calculates the wind force on an impurity from the rate of momentum transfer by electrons to the impurity, obtained as a sum over all states weighted by the distribution function,

$$\bar{F}_w^{(i)} = \sum_k \frac{\bar{k}}{\tau_i} g_k \quad (3)$$

where τ_i is the relaxation time (in principle k -dependent) due to scattering of the charge carriers by the impurity, and g_k is the non-equilibrium distribution function.⁹ The latter is obtained from solving the Boltzmann equation in the presence of an electric field \bar{E} , and reads

$$g_k = -\tau_i e \bar{v}_k \bar{E} \delta(\varepsilon_k - \varepsilon_F), \quad (4)$$

where now τ_i is the relaxation time due to all scattering processes, and \bar{v}_k is the velocity of state \bar{k} , defined as $\nabla_k \varepsilon_k$. Substituting Eq. (4) into Eq. (3) above, we obtain

$$\bar{F}_w^{(i)} = -\sum_k e \frac{\tau_i}{\tau_i} \bar{k} (\bar{v}_k \cdot \bar{E}) \delta(\varepsilon_k - \varepsilon_F), \quad (5)$$

and if we now assume that the conditions are such that the Fermi level in graphene is close to the neutrality point, so that we are in the region of the band structure where the dispersion is conical, then we have

$$\varepsilon_k = \pm v_F k, \quad (6)$$

where $v_F = 3ta/2$ is the Fermi velocity, with $a \approx 1.42 \text{ \AA}$ and t is the nearest-neighbour hopping matrix element, with a value typically taken as 2.7 eV. The plus or minus sign in Eq. (7) corresponds to the cases of n - or p -type doping, respectively. From this we can easily derive \bar{v}_k :

$$\bar{v}_k = \nabla_k \varepsilon_k = \pm v_F \frac{\bar{k}}{k}. \quad (7)$$

Substituting Eq. (7) into Eq. (5) and assuming n -type doping, we obtain

$$\bar{F}_w^{(i)} = -ev_F \sum_k \frac{\tau_\perp}{\tau_i} \bar{k} \left(\frac{\bar{k} \cdot \bar{E}}{k} \right) \delta(\varepsilon_k - \varepsilon_F). \quad (8)$$

The quotient of relaxation times appearing in Eq. (8) above can be written in terms of a quotient of mobilities: on the one hand we have that $\sigma = e\mu n$, while in graphene we also have that $\sigma = 2e^2 \sqrt{\pi} n v_F \tau$, and so we can write $\tau_\perp/\tau_i = \mu/\mu_i$, where μ is the mobility of the device, and μ_i is the mobility associated to the presence of the impurity experiencing the wind force.

We now assume that the electric field \bar{E} is directed along the z axis (see **Figure S3**), and focus on the force component parallel to the electric field, namely $F_{wz}^{(i)}$ in the geometry illustrated in **Figure S3** (it is easily shown that the other force components are zero), and change the sum over to an integration:

$$\sum_k \rightarrow \frac{gA}{4\pi^2} \int d\bar{k} \quad (9)$$

Here $g = 4$ is the degeneracy, which takes into account spin and the fact that within the Brillouin zone of graphene actually there are two cones, one at K and another one at K' , and A is the area of the graphene layer. Since in graphene the Fermi surface close to the neutrality point is a circle, it will be more convenient to work in polar coordinates. Eq. (8) is then easily summed, to obtain

$$F_{wz}^{(i)} = -\frac{e\mu E_z k_F^2 A}{\pi\mu_i} = -\frac{n\mu A}{\mu_i} eE_z, \quad (10)$$

where we have taken into account that $k_F = \sqrt{\pi n}$ for graphene. This last expression is the wind force on a single impurity; the total wind force is obtained by summing over the number of impurities, and thus we obtain

$$F_{wz} = -\frac{n\mu}{n_i\mu_i}eE_z \quad (11)$$

where n_i is the surface density of impurities; Eq. (11) is Equation 1 of our paper.

_[1] P. Ordejón, E. Artacho, and J. M. Soler, *Phys. Rev. B* **1991**, 53, R10441

_[2] J. M. Soler, E. Artacho, J. D. Gale, A. García, J. Junquera, P. Ordejón, and D. Sánchez-Portal, *J. Phys.: Condens. Matter* **2002**, 14, 2745

_[3] E. Artacho, E. Anglada, O. Dieguez, J. D. Gale, A. García, J. Junquera, R. M. Martin, P. Ordejón, J. M. Pruneda, D. Sánchez-Portal, and J. M. Soler, *J. Phys.: Condens. Matter* **2008**, 20, 064208

_[4] N. Troullier and J. L. Martins, *Phys. Rev. B* **1991**, 43, 1993

_[5] J. P. Perdew, K. Burke and M. Ernzerhof, *Phys. Rev. Lett.* **1996**, 77, 3865

_[6] G. Kresse and D. Joubert, *Phys. Rev. B* **1999**, 59, 1758

_[7] M. Brandbyge, J.-L. Mozos, P. Ordejón, J. Taylor, and K. Stokbro, *Phys. Rev. B* **2002**, 65, 165401

_[8] M. Brandbyge, K. Stokbro, J. Taylor, J. L. Mozos and P. Ordejón, *Phys. Rev. B* **2003**, 67, 193104

_[9] R. S. Sorbello, *Phys. Rev. B* **1989**, 39, 4984